HIPPOCAMPUS 26:763–778 (2016)

Activation of Local Inhibitory Circuits in the Dentate Gyrus by Adult-Born Neurons

Liam J. Drew,[1,2] Mazen A. Kheirbek,[1,2,3] Victor M. Luna,[1,2] Christine A. Denny,[1,2] Megan A. Cloidt,[2] Melody V. Wu,[1,2] Swati Jain,[4] Helen E. Scharfman,[4,5,6,7] and René Hen[1,2,3,8]*

ABSTRACT: Robust incorporation of new principal cells into pre-existing circuitry in the adult mammalian brain is unique to the hippocampal dentate gyrus (DG). We asked if adult-born granule cells (GCs) might act to regulate processing within the DG by modulating the substantially more abundant mature GCs. Optogenetic stimulation of a cohort of young adult-born GCs (0 to 7 weeks post-mitosis) revealed that these cells activate local GABAergic interneurons to evoke strong inhibitory input to mature GCs. Natural manipulation of neurogenesis by aging—to decrease it—and housing in an enriched environment—to increase it—strongly affected the levels of inhibition. We also demonstrated that elevating activity in adult-born GCs in awake behaving animals reduced the overall number of mature GCs activated by exploration. These data suggest that inhibitory modulation of mature GCs may be an important function of adult-born hippocampal neurons.

KEY WORDS: adult neurogenesis; dentate gyrus; hippocampus; granule cells; inhibition; optogenetics; interneurons

[1] **Department of Psychiatry, Columbia University, New York, NY;** [2] **Division of Integrative Neuroscience, New York State Psychiatric Institute, New York, NY;** [3] **Department of Neuroscience, Columbia University, New York, NY;** [4] **Center for Dementia Research, Nathan Kline Institute for Psychiatric Research, 140 Old Orangeburg Rd., Bldg. 35, Orangeburg, NY;** [5] **Department of Child and Adolescent Psychiatry, New York University, Langone Medical Center, New York, NY;** [6] **Department of Physiology and Neuroscience, New York University, Langone Medical Center, New York, NY;** [7] **Department of Psychiatry, New York University, Langone Medical Center, New York, NY;** [8] **Department of Pharmacology, Columbia University, New York, NY**

Additional Supporting Information may be found in the online version of this article.

Liam J Drew is currently at Division of Medicine, UCL, Gower Street, London WC1E 6BT, UK

Melody V. Wu is currently at Cold Spring Harbor Laboratory, Cold Spring Harbor, NY

Grant sponsor: NYSTEM C026430 from the New York State Stem Cell Initiative (to H.E.S., R.H.); Grant sponsor: NIH grant; Grant number: R01 NS-081203 (to H.E.S., R.H., L.J.D.); Grant sponsor: Kavli Foundation Post-Doctoral Fellowship (to L.J.D.); Grant sponsor: NIMH grant; Grant number: K01 MH-099371 (to M.A.K.); Grant sponsor: NYS Office of Mental Health (to H.E.S., R.H.).

Abreviations used: DCX, doublecortin; DG, dentate gyrus; EE, enriched environments; GC, granule cell; GFP, green fluorescent protein; IEG, immediate early gene; IR-DIC, infrared-differential interference contrast; PBS, phosphate buffered saline; PFA, paraformaldehyde; POMC, proopiomelanocortin; PV, parvalbumin; SH, standard housing; TMX, Tamoxifen.

*Correspondence to: René Hen, NYSPI, Kolb Research Annex, 1051 Riverside Drive, Unit 87, New York, NY 10032. E-mail: rh95@cumc.columbia.edu

Accepted for publication 7 December 2015.

DOI 10.1002/hipo.22557

Published online 14 December 2015 in Wiley Online Library (wileyonlinelibrary.com).

INTRODUCTION

In the adult mammalian brain, the dentate gyrus (DG) is unique in continuously incorporating newly born principal neurons into pre-existing circuitry (Zhao et al., 2008; Ming and Song 2011; Drew et al., 2013). Most work aimed at determining the functions of adult-born GCs has focused on the idea that they encode and transfer entorhinal cortical input to hippocampal area CA3 in a way that is distinct from mature, perinatally born GCs (Wang et al., 2001; Ge et al., 2007; Mongiat et al., 2009; Gu et al., 2012; Marín-Burgin et al., 2012). Such studies have mainly presented adult-born neurons as functioning in parallel to and independently of the significantly larger population of mature GCs.

Principal neurons, however, in addition to conveying information to downstream structures, influence local processing via projections to neighboring interneurons and/or principal neurons (Isaacson and Scanziani, 2011). Dentate GCs are not reciprocally connected but the region contains a network of different neuronal classes, including glutamatergic mossy cells (Scharfman and Myers, 2013) and numerous GABAergic cell types (Houser, 2007). GC axons, *en route* to CA3, form collateral synapses onto glutamatergic and GABAergic neurons in the hilus that project back to GCs, suggesting that both feedback inhibition (Sambandan et al., 2010) and excitation (Scharfman, 1995a) significantly influence DG processing and its ultimate output to CA3.

Axons of immature adult-born GCs branch considerably in the hilus (Ide et al., 2008; Toni et al., 2008; Sun et al., 2013) and functional inputs from mature 3-4-month-old adult-born neurons onto hilar neurons have been reported (Toni et al., 2008). Ablating adult neurogenesis increases the amplitude of gamma bursts in the DG (Lacefield et al., 2012) implicating adult-born neurons as key regulators of local networks of GABAergic

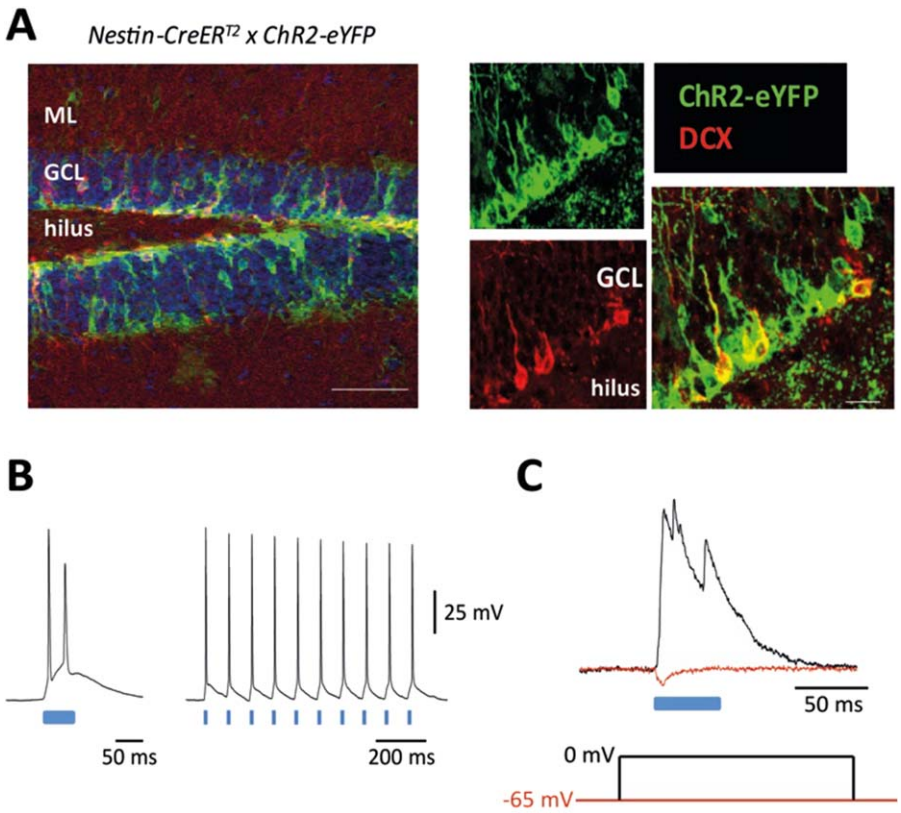

FIGURE 1. ChR2 expression in adult-born GCs and optically evoked synaptic input to mature GCs. A: *Left*, Image of the DG showing expression of ChR2-eYFP (green) and DCX (red) in a mouse 7 weeks after TMX-induced recombination. Scale bar: 100 µm. *Middle*, eYFP and DCX immunoreactivity at higher magnification. *Right*, co-expression of these proteins in young neurons. DCX expression terminates ≈3 weeks post-mitosis so older abGCs show only as green. Scale bar: 15 µm. B: *Left*, firing in a ChR2-eYFP-expressing neuron in response to a 50 ms light pulse. *Right*, Response to 2 ms pulses at 10 Hz. C: *Bottom*, voltage-clamp protocol for isolating GABAergic and glutamatergic currents each recorded at the reversal potential of the other. *Top*, example IPSC (*black*) and EPSC (*red*).

interneurons that modulate mature GC activity. This idea is also supported by a study in which increasing or decreasing adult neurogenesis impacted overall DG excitability in *ex vivo* slices (Ikrar et al., 2013) potentially via effects on local inhibition.

In this study, we focused on adult-born GCs up to 6–7 weeks of cellular age, because adult-born neurons have been shown to make significant contributions to cognitive processing when they are between 4 and 6 weeks post-mitosis (Denny et al., 2012; Swan et al., 2014). To determine if this cohort of adult-born GCs generate network-mediated synaptic input to mature GCs, we expressed channelrhodopsin-2 (ChR2) selectively in them to allow for their optical stimulation. Light-evoked synaptic inputs were observed onto mature GCs in hippocampal slices, and they were dominated by GABA-mediated inhibition. Optical stimulation of adult-born GCs *in vivo* decreased the number of mature GCs activated by exploration of a novel environment indicating a net inhibitory effect on the DG of activating these neurons. Together these data suggest that adult-born neurons in the hippocampus modulate mature GCs by regulating local inhibitory circuits.

RESULTS

ChR2 was targeted to adult-born GCs by crossing a floxed-stop ChR2-enhanced yellow fluorescent protein (eYFP) mouse line (Ai32;, Madisen et al., 2012) to a Nestin-CreER^{T2} line (Dranovsky et al., 2011) (henceforth, Nestin-ChR2 mice, Supporting Information Fig. S1a). When mice were 6–8 weeks of age, recombination was induced in Nestin-expressing neural stem cells, so that all neurons arising from modified stem cells expressed ChR2-eYFP, i.e., a population of ChR2-expressing adult-born GCs of various ages (0 to time-after-induction) was created (Fig. 1a). Whole-cell recordings from ChR2-eYFP-expressing neurons showed that blue light pulses depolarized them to evoke action potential firing (Fig. 1b).

Experiments were performed 6–7 weeks after ChR2-induction to study a population of adult-born neurons in their early stages of maturation before they assume a mature phenotype; during this period the neurons' physiological properties differ significantly from mature GCs (see Zhao et al., 2008;

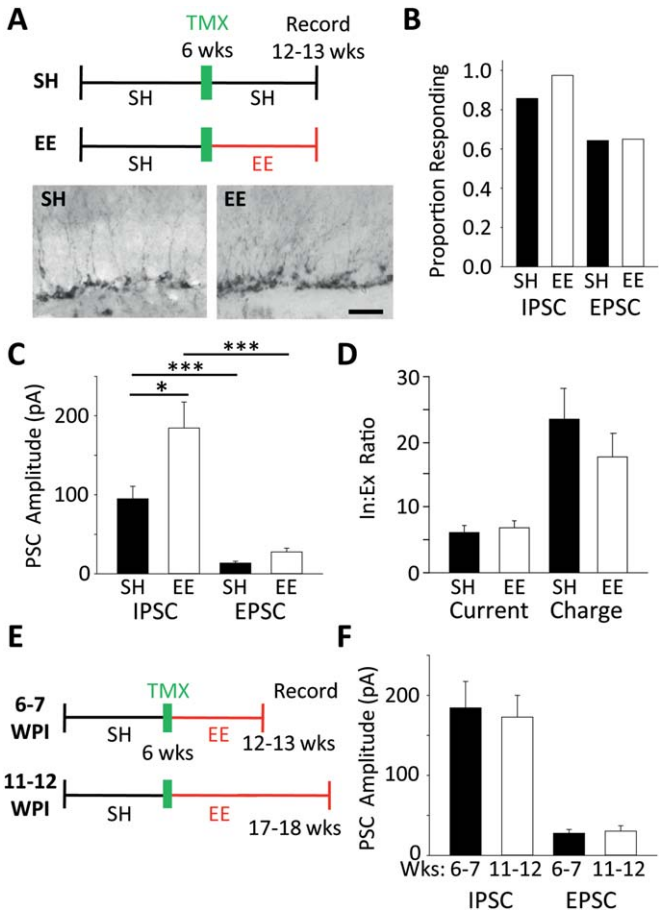

FIGURE 2. Activation of adult-born GCs evoked strong synaptic input to mature GCs that is augmented by environmental enrichment and is saturated by 6–7 weeks post-mitosis. A: *Top*, Experimental timeline. *Bottom*, typical images of DG DCX immunoreactivity in mice from SH (*left*) and EE (*right*). Scale bar: 50 µm. B: Similar proportions of neurons from SH and EE mice displayed IPSCs ($P = 0.15$) and EPSCs ($P = 1.0$, Fisher's exact test). C: Mature GCs from EE mice had larger IPSCs than those from SH (EE: 184.4 ± 33.0 pA vs. SH: 94.9 ± 15.8 pA; Mann-Whitney Ranked Sum, $P = 0.036$). There was a trend for larger EPSCs in EE animals (EE: 27.7 ± 4.7 pA vs. SH: 13.6 ± 2.3 pA; Mann-Whitney Ranked Sum, $P = 0.068$). D: EE did not impact the dominance of inhibition. I:E ratios for peak current (EE: 6.7 ± 1.2 vs. SH: 6.2 ± 1.0; t-test, $P = 0.74$) and for charge transfer (EE: 17.7 ± 3.6 vs. SH: 23.3 ± 4.9; t-test, $P = 0.81$). E: Experimental timeline; optically evoked synaptic input was recorded either 6–7 or 11-12 weeks post-induction (WPI). F: There was no significant difference in the amplitudes of either IPSCs or EPSCs recorded at the respective time points. (IPSCs: 6–7 weeks (n =40): 184.4 ± 33.0 pA vs. 11–12 weeks ($n = 15$): 172.9 ± 27.1 pA; Mann-Whitney Ranked Sum, $P = 0.58$. EPSCs: 6–7 weeks ($n = 40$): 27.7 ± 4.7 pA vs. 11–12 weeks ($n = 11$): 30.3 ± 6.7 pA; Mann-Whitney Ranked Sum, $P = 0.47$.).

Ming and Song 2011; Drew et al., 2013) and they make specific contributions to cognition (Denny et al., 2012; Gu et al.,2012; Drew et al., 2013). Immunohistochemical analysis showed that 85.4 ± 1.5% of cells expressing doublecortin (DCX) (a marker of immature neurons) contained ChR2-eYFP, indicative of high recombination rates (Fig. 1a). The ChR2-eYFP population contained markers for multiple stages of neuronal maturation further confirming that the ChR2-eYFP-positive cells assume neuronal fates (see Supporting Information Figs. S1b,c). Consistent with Nestin's expression profile, neural stem cells expressed ChR2-eYFP and their tufts were clearly identifiable throughout the GCL and frequently in the inner molecular layer (Supporting Information Fig. S2).

To test our hypothesis (Supporting Information Fig. S1d), that adult-born GCs excite local circuit neurons that synapse onto the much larger population of mature developmentally born GCs in the DG (henceforth, mature GCs), we made whole-cell recordings from mature GCs and optically activated the population of 0 to 6–7 week old adult-born GCs. Pulses of blue light elicited synaptic currents in nearly all mature GCs (Fig. 1c), consistent with adult-born GCs ≤6 weeks-old being sufficiently well connected to activate local neurons that innervate mature GCs.

We examined synaptic responses in slices from mice kept under standard housing conditions (SH) and mice housed in enriched environments (EE). Environmental enrichment increases the number of adult-born neurons in the DG two- to fivefold (see Dranovsky et al., 2011 plus Kempermann et al., 1997; van Praag et al., 1999; Bruel-Jungerman et al., 2005;) consistent with representative sections examined in this study (Fig. 2a). Inhibitory (GABAergic) and excitatory (glutamatergic) postsynaptic currents (IPSCs and EPSCs, respectively) in mature GCs were measured separately (Fig. 1c, Supporting Information Fig. S1e for pharmacological confirmation) and the balance of the two was assessed. In slices from SH mice, 85.7% of mature GCs (24 of 28) displayed IPSCs (Fig. 2b) with an average peak amplitude of 94.9 ± 15.8 pA (Fig. 2c). Conversely, 64.3% cells (18 of 28 cells) displayed a relatively small EPSC with an average peak amplitude of 13.6 ± 2.3 pA (Figs. 2b,c). EPSCs recorded at −65 mV persisted in the presence of the $GABA_A$ receptor antagonist SR95531 ($n = 5$) indicating that synaptic events recorded at this holding potential were not GABAergic currents (data not shown.) The ratio of peak IPSC to EPSC amplitude showed that inhibition was approximately six-fold greater than excitation (Fig. 2d). Typically, however, IPSCs evoked by 50 msec light pulses were complex events with multiple peaks whereas EPSCs were single monophasic events (see Supporting Information Figs. 1c, 3f, 4a, 5e) and measuring total charge transfer over 50 msec for GABAergic and glutamatergic inputs showed that inhibition dominated excitation by over 20-fold (Fig. 2d).

Consistent with augmented neurogenesis, mature GCs from EE-housed Nestin-ChR2 mice displayed approximately twice the level of optically evoked inhibition; the peak amplitude of IPSCs increased to an average of 184.4 ± 33.0 pA ($n = 40$, $P = 0.036$, vs. 94.9 ± 15.8 pA for SH, $n = 28$ Fig. 2c) with 39 of 40 neurons demonstrating an IPSC ($P = 0.15$ vs. SH, Fig. 2b). Following enrichment there was a trend toward EPSCs being larger, but this was not statistically significant (EE: 27.7 ± 4.7 pA vs. SH: 13.6 ± 2.3 pA, $P = 0.068$, Fig. 2c).

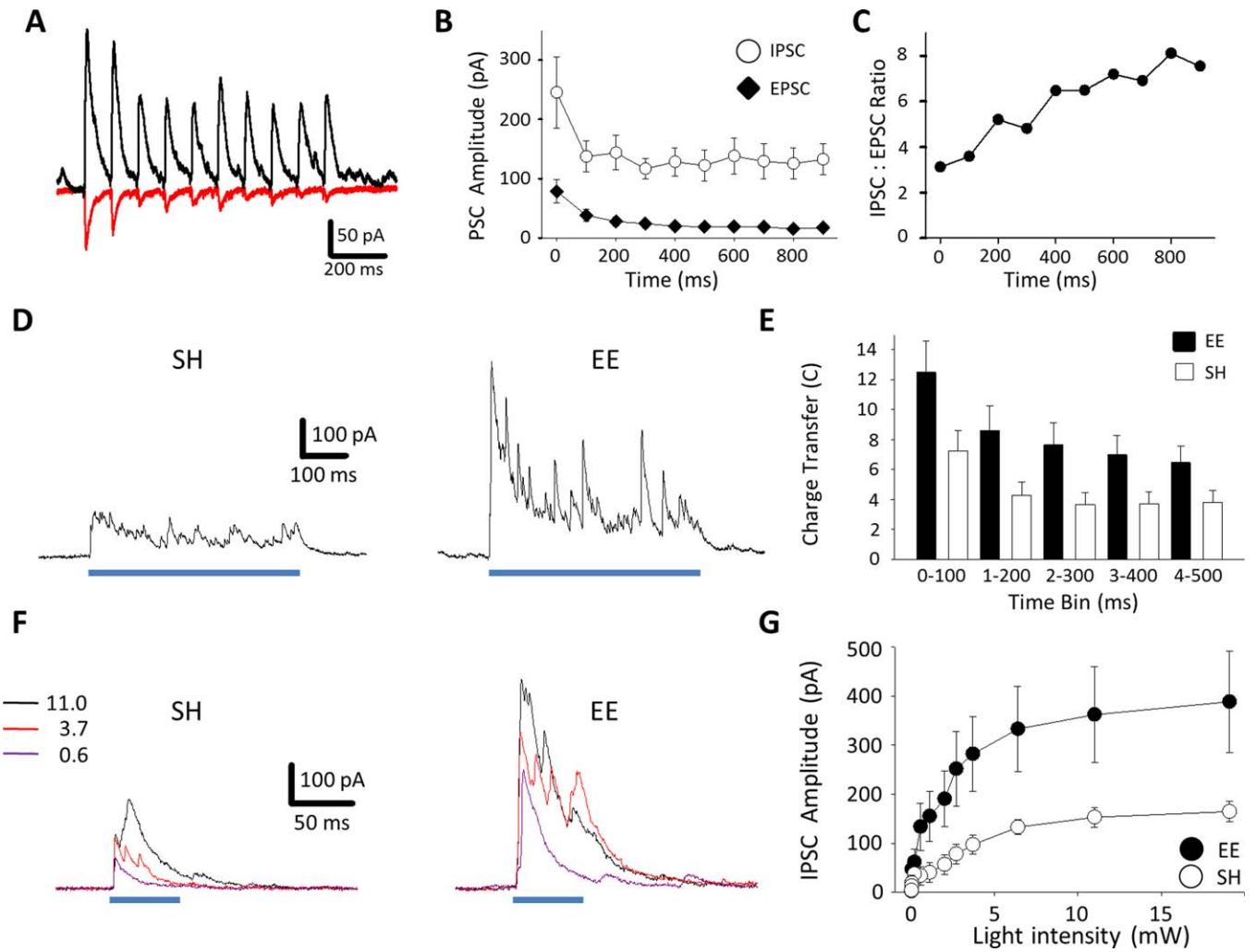

FIGURE 3. Dynamic properties of optically evoked synaptic currents. A: Example traces of IPSCs (*black*) and EPSCs (*red*) evoked by 10 Hz trains of 2 ms light pulses. B: During 10 Hz trains both IPSCs and EPSCs depressed with repeated stimulation; the ratio of the EPSCs elicited by the 10th and 1st stimuli was 0.22, showing greater depression than IPSCs (mean 10^{th}:1^{st}: 0.54, $n = 10$). C: The ratio of the mean IPSC:EPSC amplitude progressively increased during 10 Hz stimulation. D: Example traces of optically evoked IPSCs at different light intensities (in mW, as indicated.) *Left*, SH mouse; R*ight*, EE animal. E: IPSCs increase with light intensity in both EE ($n = 5$) and SH ($n = 6$; 2-way, RM ANOVA: Effect of light: $F_{(11,\ 99)} = 21.05$, $P < 0.001$; effect of housing: $F_{(1,\ 9)} = 16.43$, $P = 0.032$; interaction: $F_{(11,\ 99)} = 4.05$, $P < 0.001$). F: Example traces of IPSCs evoked by 500 ms light pulses from an SH mouse (*left*) and an EE mouse (*right*). G: Time course of synaptic input over sustained illumination in EE and SH neurons. There was a significant effect of time but housing alone did not reach significance (2-way, RM ANOVA: effect of time interval, $F_{(4,\ 84)} = 6.48$, $P < 0.001$; effect of housing, $F_{(1,\ 21)} = 2.25$, $P = 0.15$; interaction, $F_{(4,\ 84)} = 5.13$, $P < 0.001$).

There was no change in the proportion of cells with EPSCs (26/40, $P = 1.0$ vs. SH, Fig. 2b). These changes indicated that following EE the ratio of GABAergic to glutamatergic input still heavily favored inhibition (Fig. 2d).

When we recorded synaptic inputs to mature GCs in Nestin-ChR2mice 11-12 weeks after transgene induction (Fig. 2e), so that the population of optically activated neurons included a large fraction of mature adult-born neurons well-beyond their critical periods (see Drew et al., 2013), neither IPSCs nor EPSCs were larger than after 6–7 weeks post-induction (Fig. 2f). This suggests that activation of local circuits (in the slice preparation, at least) is relatively saturated by 6–7 weeks post-induction and that there is no major up-regulation of inhibitory recruitment by adult-born GCs as they develop beyond this critical period. (All subsequent experiments looked 6–7 weeks post-induction.)

Using 2 ms light pulses to restrict stimulated adult-born GCs to single spikes, we next confirmed that the activated adult-born GC-to-mature GC circuitry could follow physiologically relevant firing rates (based on *in vivo* electrophysiological studies; Leutgeb et al., 2007; Neunuebel and Knierim, 2012). Thus, in a new cohort of EE mice, 10 Hz optical stimulation

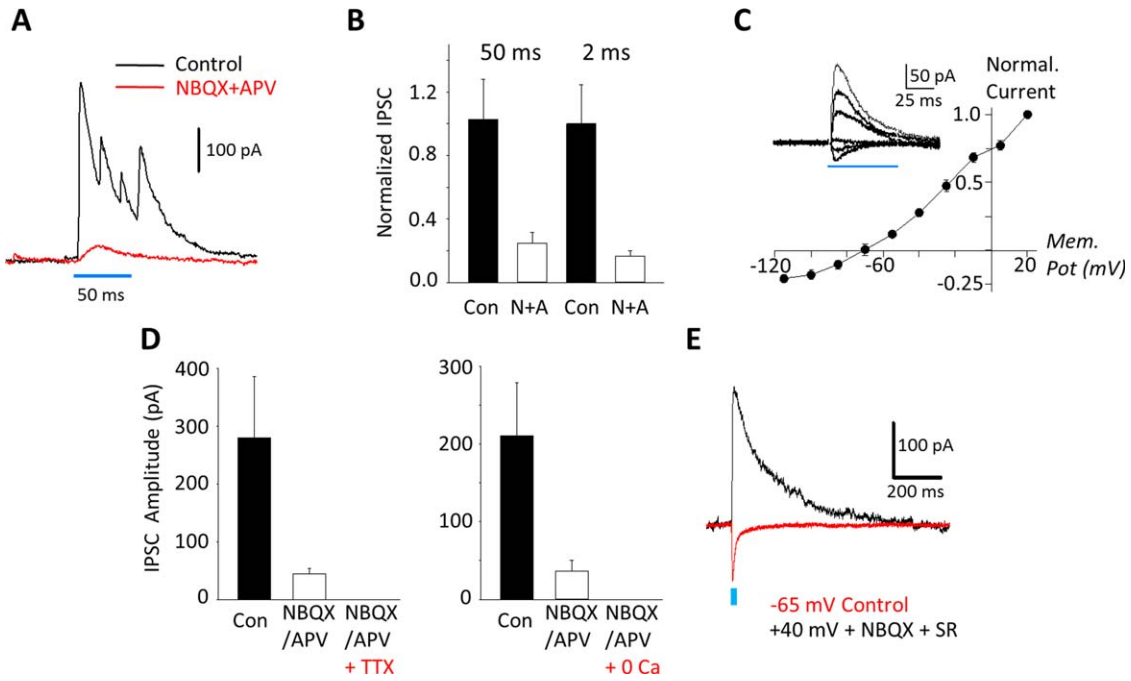

FIGURE 4. Evidence for direct neurotransmission from adult-born GCs to mature GCs. A: Example traces of optically evoked IPSCs, before (*black*) and after (*red*) application of glutamate antagonists (10 μM NBQX, 100 μM DL-APV). B: NBQX/APV reduced IPSC amplitudes evoked by 50 ms stimuli by 75.1 ± 6.6% (Control: 199.6 ± 48.8 pA, NBQX/APV: 38.2 ± 13.0 pA, $n = 14$; Paired t-test, $P < 0.001$) and by 2 ms stimuli (in a distinct cohort of cells) by 76.0 ± 6.4% (Control mean: 245.3 ± 60.2 pA, residual mean: 40.7 ± 8.2 pA, $n = 10$; Wilcoxon Signed Rank Test, $P = 0.002$). C: Current-voltage relationship for residual currents (after NBQX+APV application, $n = 8$, currents normalized to peak amplitude at +20mV). *Inset*, IPSCs evoked at −115, −85, −55, −25, +5 and +20 mV holding-potentials. D: Residual IPSCs were abolished by 1 μM TTX (*left*, $n = 5$) and by nominal 0 mM extracellular calcium (*right*, $n = 5$). E: Representative trace of a an NMDA receptor-mediated current recorded at +40 mV (*black*) following blockade of AMPA and $GABA_A$ receptors, 5/5 cells tested showed such currents (mean amplitude: 190.3 ± 28.1 pA). For comparison, an AMPA receptor-mediated current at −65 mV in control conditions is shown. The 2 forms of glutamatergic input did not correlate in amplitude (Spearman Rank Correlation, $r^2 = 0.6$, $P = 0.35$, $n = 5$).

showed that both IPSCs and EPSCs followed this frequency (Figs. 3a,b). Dominance of inhibition over excitation was again evident on the first stimulus (IPSC: 245.3 ± 60.2 pA; EPSC: 78.7 ± 19.9 pA; $P = 0.009$, mean I:E ratio: 5.9 ± 2.3, $n = 10$; Fig. 3b). In addition, despite both inputs depressing during stimulus trains, EPSCs did so more than IPSCs (EPSCs: mean ratio, 10th:1st = 0.22; IPSCs: 10^{th}:1^{st} = 0.54, Fig. 3b). Therefore, sustained activity in adult-born GCs shifts the relative balance of inputs to mature GCs further in favor of inhibition (Fig. 3c).

As recruitment of GABAergic input was the major effect of stimulating adult-born GCs, IPSCs were characterized further. IPSCs in response to 10 Hz stimulation showed similar dynamics in slices from both SH and EE animals (i.e. an initial depression followed by stable IPSC amplitudes, Supporting Information Fig. S3a). Moreover, recordings in slices from EE mice showed that IPSCs also robustly followed 20 Hz stimulation (Supporting Information Fig. S3b). Varying the optical stimulus duration (from 0.5 to 50 ms) showed a minor effect on IPSC peak amplitude (Supporting Information Fig. S3c) but a pronounced effect on total charge transfer as synaptic events became more complex, presumably reflecting repeated firing in adult-born GCs and target interneurons (Supporting Information Fig. S3c). When stimuli were prolonged to 500 ms IPSCs continued throughout (Figs. 3d,e, Supporting Information Fig. S3d).

We then reasoned that if light power was decreased, progressively fewer adult-born GCs would be activated, so we measured how IPSCs changed with light power. As predicted IPSCs in mature GCs became smaller with decrementing light intensity (Figs. 3f, g, Supporting Information Fig. S3e) but importantly IPSCs were elicited even at low light power (< 1 mW) and they increased linearly with light intensity up to approximately 7 mW (Fig. 3g). These data suggest that rather than a cohort of adult-born neurons together activating a powerful inhibitory network in an all-or-none manner, individual adult-born neurons make discrete contributions to a graded inhibitory response.

Next, we addressed the hypothesized disynaptic circuit mediating inhibition (Supporting Information Fig. S1d). If an adult-born GC-to-inhibitory neuron-to-mature GC circuit were fundamental, glutamate receptor antagonists, acting at the first synapse, would abolish optically evoked IPSCs onto mature GCs. Indeed, blocking AMPA and NMDA receptors

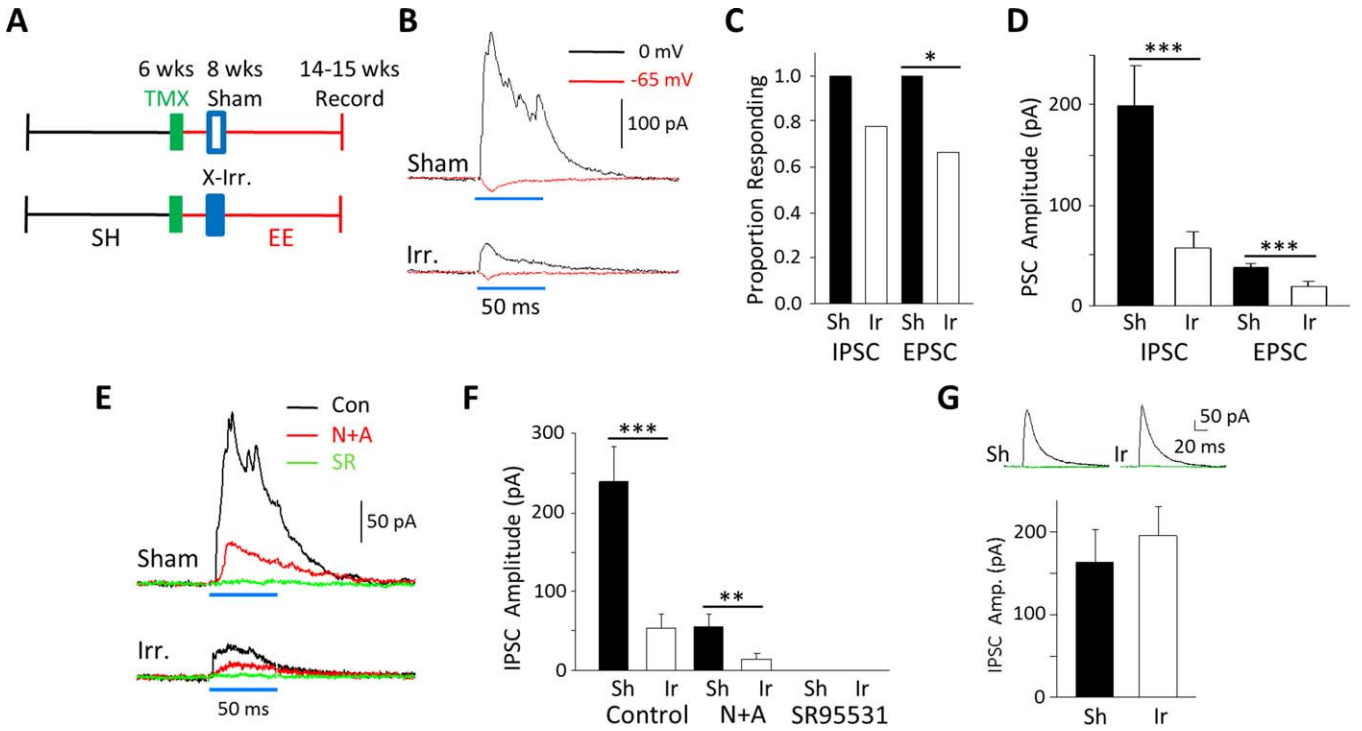

FIGURE 5. Effect of hippocampal X-irradiation on optically evoked responses. A: Experimental timeline. B: Example traces of an IPSC (*black*) and an EPSC (*red*) from a sham-treated mouse (*top*) and an irradiated mouse (*bottom*). C: Fewer mature GCs displayed synaptic currents following irradiation and this was statistically significant for EPSCs (Sham: 1.0 (16/16) vs. X-ray: 0.67 (12/18, Fisher's Exact Test, $P = 0.020$) but not IPSCs (Sham: 1.0 (16/16) vs. X-ray: 0.78 (14/18, $P = 0.11$). D: The average synaptic current for both inhibition and excitation was significantly reduced by irradiation: IPSCs by 71.3% (Sham: 198.7 ± 39.7 pA, $n = 16$, vs. X-ray: 57.0 ± 16.7 pA, $n = 18$; Mann-Whitney Ranked Sum, $P < 0.001$) and EPSCs by 53.3% (Sham: 37.5 ± 4.8 pA, $n = 16$, vs. X-ray: 17.5 ± 6.0 pA, $n = 18$; Mann-Whitney Ranked Sum, $P < 0.001$). E: Example traces of IPSCs in control ACSF (*black*), plus NBQX/APV (*red*) and NBQX/APV/SR 95531 (*green*) from a sham (*top*) and an X-irradiated mouse (*bottom*). F: IPSCs in control conditions were larger in sham than in X-irradiated animals (Sham: 227.3 ± 43.0, $n = 11$, vs. X-ray: 53.0 ± 18.6 pA, $n = 17$; Mann-Whitney Ranked Sum, $P < 0.001$). Residual IPSCs evoked in APV/NBQX are 75.9% smaller in irradiated animals than in shams (Sham: 60.6 ± 15.8, $n = 11$, vs. X-ray: 14.6 ± 6.2 pA, $n = 17$; Mann-Whitney Ranked Sum, $P < 0.001$). All currents were abolished by SR 95531. G: Electrically evoked IPSCs did not significantly differ between groups (Sham: 163.0 ± 40.6 pA, $n = 14$, vs. X-ray 195.0 ± 36.1 pA, $n = 17$; Mann-Whitney Ranked Sum, $P = 0.46$). *Inset*, example traces in ACSF (*black*) and in 10 µm SR 95531 (*green*).

substantially reduced light-activated IPSCs indicating that three fourths of inhibition is mediated by such a disynaptic circuit. Surprisingly, however, a small residual IPSC remained (Fig. 4a). Using both 50 ms and 2 ms light stimuli the residual GABAergic current corresponded to approximately 25% of the control peak IPSC (Fig. 4b) with 18/24 mature GCs displaying such a response. Residual currents had an IV curve characteristic of $GABA_A$ receptors (Fig. 4c) and were blocked by the $GABA_A$ antagonist SR 95531 (see Fig. 5f). They also appeared dependent on conventional vesicular release, as they were ablated by blocking sodium channels with tetrodotoxin and by reducing extracellular calcium to nominally 0 mM (Fig. 4d). Hence, these IPSCs suggested that stimulation of abGCs led to direct release of GABA onto mature GCs.

Various investigations have provided evidence that during development immature GCs co-release GABA and glutamate before they establish a mature glutamatergic phenotype (Walker et al., 2001; Gutiérrez, 2005; Beltrán and Gutiérrez, 2012). Therefore, we investigated if a direct glutamatergic input was also observable. To test for this we blocked AMPA receptors to prevent adult-born GCs from synaptically exciting postsynaptic neurons and blocked $GABA_A$ receptors with SR 95531 to record NMDA receptor-mediated currents at positive potentials; in five of five mature GCs tested, we observed NMDA receptor activation (Fig. 4e).

The latency from light onset to residual IPSC should, we hypothesized, help indicate a mono- or disynaptic route. We therefore compared latency to IPSC onset with Cre-lines that targeted ChR2 to either parvalbumin (PV)-expressing interneurons that directly innervate mature GCs or to mature GCs that would evoke disynaptic inhibition, however latencies in Nestin-ChR2 mice were highly variable (Supporting Information Figs. S4a–d). Interestingly, latencies remained similar (and hence highly variable, Supporting Information Fig. S4c) when glutamatergic recruitment of interneurons was blocked suggesting that a monosynaptic IPSC determined the latency. In the

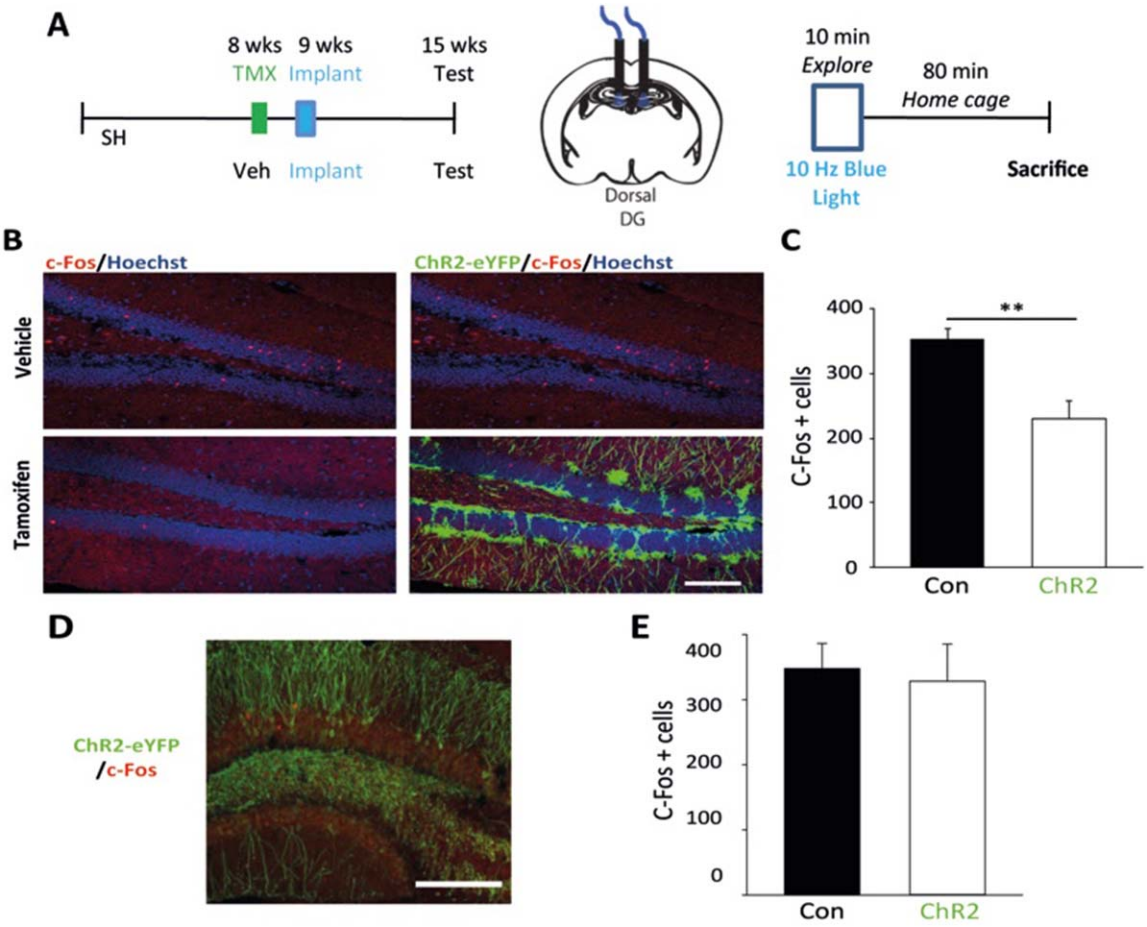

FIGURE 6. Stimulation of adult-born GCs *in vivo* reduces the number of mature GCs activated during a novel experience. A: Overall timeline of experiment (*left*), diagram showing fiber optics positioning (*center*) and timeline of final exploration session (*right*). B: Example images of c-Fos expression in the DG just ventral to the fiber optic implantation site from, *top*, a vehicle-treated animal and, *bottom*, a TMX-treated animal. Images on the *right* indicate presence or absence of ChR2-eYFP expression. Scale bar = 100 μm. C: ChR2-induction reduced the number of GCs immunopositive for c-Fos (number = total of 12 sections spanning the entire dorsoventral axis in one hemisphere). Control: 352.4 ± 17.6, $n = 7$, ChR2: 229.0 ± 28.9, $n = 5$; t-test, $P = 0.003$. D: Example image of ChR2-eYFP expression (green) in an Arc-ChR2 mouse with immunohistochemical labeling of c-Fos (red). E. Quantification of the total number c-Fos expressing cells per hemisphere showed that activation of ChR2 expressing neurons in Arc-ChR2 mice did not significantly change total number of active DG neurons. (Control: 347.8 ± 38.5 neurons, $n = 6$ mice, ChR2: 328.4 ± 57.0, $n = 4$; t-test, $P = 0.78$).

one cell in which the initial IPSC had a long (~9 ms) latency, that IPSC was entirely abolished by NBQX/APV. It also, therefore, suggests that the mixed latencies of inputs result from factors intrinsic to the adult-born neurons (i.e., are not dependent on circuit properties), this is potentially related to immature firing and transmitter release properties of adult-born cells and/or an involvement of volume transmission of GABA from ChR2-expressing cells.

Given these results and that concerns have been raised about the specificity of Cre-recombinase activity in Nestin-CreER^{T2} mice—albeit Cre activity varied with the reporter gene employed (Sun et al., 2014)—we sought to further confirm that in Nestin-ChR2 mice transgene expression was confined to adult-born GCs. First, we compared ChR2-eYFP labeling with immunoreactivity for glutamic acid decarboxylase-67 (GAD67) and PV, markers for GABAergic interneurons generally and for fast-spiking basket cells, respectively. In three mice (three sections per animal) we did not find ChR2-eYFP expression in any GAD67- (Supporting Information Fig. S5a, 0/316 cells) or PV-expressing (Supporting Information Fig. S5b, 0/101 cells) neurons. Next, we labelled sections for eYFP and calretinin, a marker in the hilus of mossy cells, and some interneurons, and found no hilar co-expression with ChR2-eYFP (Supporting Information Fig. S5c, 0/224 cells). Overall, these data support specific expression of ChR2 in adult-born GCs and neural stem cells in the DG, with little or no off-target expression, and suggest that the small number of hilar neurons sometimes seen to contain ChR2-eYFP in Nestin-ChR2 mice may be ectopic adult-born neurons (McCloskey et al., 2007; Myers et al., 2013).

To complement these data, we also tested the critical role of adult-born GCs in mediating the observed synaptic currents by recording optically evoked events in two sets of mice where neurogenesis was substantially reduced—aged mice and X-irradiated mice.

Adult hippocampal neurogenesis decreases significantly with age in rodents (Klempin and Kempermann, 2007). Here, neurogenesis (as assessed by DCX staining) in 35 week-old mice was strikingly low (Supporting Information Figs. S6a, b) consistent with reports of dramatic decreases by 5 months of age (to ~5% of levels at 6 weeks, Denny et al., 2012). Therefore, we determined if there was a parallel drop in optically evoked synaptic currents. IPSCs in mature GCs of animals that were 7 months-old at the time of induction were substantially smaller than those from 2 month-old mice induced and housed in parallel (Supporting Information Figs. S6c, d). Hence, all mature GCs from control (SH) 14 week-old mice displayed IPSCs (12/12) and had an average amplitude of 84.1 ± 20.2 pA (Supporting Information Fig. S6d), whereas in 35 week-old (SH) animals only 41.7% of cells displayed IPSCs (5/12, $P = 0.0046$, Supporting Information Fig. S6c) and the overall amplitude was substantially lower, 13.2 ± 2.7 pA ($P < 0.001$, Supporting Information Fig. S6d). Surprisingly however, EPSCs were not affected by aging ($P = 0.19$, Supporting Information Fig. S4c, d), hence a dominance of inhibition over excitation was not observed in older animals (Supporting Information Fig. S6e).

To more specifically arrest adult neurogenesis, we focally X-irradiated the hippocampi of a cohort of EE-housed Nestin-ChR2 mice 1-2 weeks after TMX-induced recombination, to kill dividing cells and neurons <2 weeks of age (Dranosky et al., 2011; Denny et al., 2012; 2014; Fig. 5a). Then, we first measured the presence and amplitudes of light-evoked PSCs in mature GCs from sham- and X-irradiated mice (Figs. 5b–d). Following X-ray, average amplitudes of the IPSCs were reduced by 71.3% (Sham: 198.7 ± 39.7 pA, $n = 16$ vs. X-ray: 57.0 ± 16.7, $n = 18$, $P < 0.001$, Fig. 5d) and EPSCs by 53.3% (Sham: 37.5 ± 4.8 pA, $n = 16$ vs. X-ray: 17.5 ± 6.0, $n = 18$, $P < 0.001$, Fig. 5d). Fewer cells displayed any synaptic currents at all and this was statistically significant for EPSCs (IPSCs: Sham, 16/16. X-ray: 14/18, $P = 0.11$. EPSCs: 16/16. X-ray: 12/18, $P = 0.020$, Fig. 5c).

We then reasoned that if the residual IPSCs (elicited with glutamate receptors blocked; see Figs. 4a,b) are mediated directly by adult-born GCs, they too should be smaller following X-irradiation. Indeed, following application of the glutamate receptor antagonists (Figs. 5e,f), the residual IPSC was smaller by 73.8% in slices where young adult-born neurons had been ablated (Sham: 55.7 ± 16.6 pA, $n = 10$ vs. X-ray: 14.6 ± 6.2, $n = 17$, $P = 0.003$, Fig. 5f). These monosynaptic IPSCs were abolished by the $GABA_A$ antagonist SR 95531 (Figs. 5e,f). We also tested if X-irradiation had non-specific effects on inhibition by recording electrically evoked IPSCs and no difference was apparent between sham and X-irradiated groups (Fig. 5g) suggesting that inhibitory networks had been left intact. In summary, these data indicate that the majority of the disynaptic and monosynaptic effects are mediated by young adult-born GCs (Supporting Information Fig. S7).

Next, we determined whether adult-born neurons can modulate mature GCs in the intact hippocampus, hypothesising that stimulating adult-born GCs would suppress mature GC activity. As a marker of neuronal activity *in vivo*, we used immediate early gene (IEG) expression, taking advantage of the fact that exploration of a novel environment leads to sparse but robust induction of IEGs in GCs (Chawla et al., 2005). Thus, after treatment with TMX or vehicle, Nestin-ChR2 mice were bilaterally implanted with fiber optics above the dorsal DG to activate a cohort of adult-born GCs *in vivo* (Kheirbek et al., 2013; Fig. 6a, Supporting Information Fig. S8a). These animals then explored a novel arena while blue light was pulsed at 10 Hz throughout the trial period (which did not significantly impact behavior, Supporting Information Fig. S8b) and 80 minutes later they were sacrificed and their brains processed so as to quantify the number of neurons in the GCL expressing the IEG c-Fos (Figs. 6b,c, Supporting Information Fig. S8c).

Consistent with activation of adult-born GCs inhibiting mature GCs, the total number of GCs expressing c-Fos was significantly reduced by optogenetic stimulation—that is, 35.0% fewer neurons were labeled in the TMX- treated group compared to vehicle-treated controls (Vehicle: 352.4 ± 17.6 per hemisphere, $n = 7$, vs. TMX: 229.0 ± 28.9, $n = 5$, $P = 0.003$; Fig. 6c). Thus, elevating activity in adult-born GCs reduced the overall number of GCs active during behavioral exploration.

Finally, we sought to use a system in which we could genetically modify a similarly sized cohort of GCs that were predominately mature developmentally born neurons, so as to compare the effects of activating mature GCs versus young, adult-born GCs on inhibitory processing in the DG. To do so, we used Arc-$CreER^{T2}$ transgenic mice to express ChR2-eYFP in mature GCs (Denny et al., 2014; Fig. 6d). In these mice recombination is dependent on neuronal activity, hence, three weeks prior to the experiment we exposed Arc-ChR2 to a fear-conditioning protocol so as to induce ChR2-eYFP in a sparse number of GCs. Quantification of the number of ChR2-eYFP labeled neurons in the GCL showed that a remarkably similar number of GCs expressed ChR2-eYFP in Arc- and Nestin-ChR2 mice (Supporting Information Fig. S9a). Crucially, in Arc-ChR2 mice only 1.5% of DCX expressing neurons contained ChR2-eYFP (see also Stone et al., 2011) indicating that the vast majority of ChR2-positive neurons were mature GCs (data not shown, in Danielson et al., submitted). When we looked at optically evoked synaptic events (Supporting Information Figs. S9b–f) we found no significant difference in IPSC amplitudes between Arc-ChrR2 and Nestin-ChR2 mice (Arc: 134.5 ± 49.1 pA, $n = 13$; Nestin, as in Fig. 1: 184.4 ± 33.0 pA, $n = 40$, $P = 0.11$; Supporting Information Figs. S9c,d) and EPSCs in either group were similar in amplitude (Arc-ChR2: 17.7 ± 6.7 pA, $n = 13$. Nestin (as in Fig. 1): 27.7 ± 4.7 pA, $n = 40$. $P = 0.58$). IPSCs again followed 10 Hz stimulation showing similar within train depression as those evoked in Nestin-ChR2 mice (Supporting Information Fig. S9f).

We then further explored the effect of activating this sparse population of mature GCs on dentate processing *in vivo* by using the same paradigm as in the experiment in Figures 6a,d (see Supporting Information Fig. S10a). Arc-ChR2 mice, and control mice lacking the Cre-ER^{T2} allele, explored a novel environment with 10 Hz optical stimulation throughout the trial period (which had no significant effect on behavior, Supporting Information Fig. S10b) and subsequently the number of GCs expressing c-Fos was counted (Fig. S10c). In contrast to the effect of stimulating adult-born neurons, activation of a similar number of predominately mature GCs did not decrease the number of DG neurons expressing c-Fos (Fig. 6e, Supporting Information Fig. S10d). This result suggests that mature GCs do not recruit inhibitory circuits as strongly as adult-born GCs do.

DISCUSSION

To understand how adult neurogenesis contributes to hippocampal function, it is necessary to determine how adult-born GCs affect all aspects of information processing within the DG-CA3 network into which they integrate. Here we have demonstrated, using an optogenetic strategy, that activated adult-born GCs robustly recruit GABAergic interneurons that synaptically inhibit mature GCs. Consistent with their established effects on adult neurogenesis, aging, which majorly reduces adult neurogenesis in rodents, and housing in an EE, which increases the rate of neurogenesis, changed the degree of optically evoked inhibition of mature GCs in the predicted manner. These results, hence, demonstrate that recruitment of inhibition is a dynamic property of the circuit. Additionally, synaptic excitation onto mature GCs was observed following stimulation of adult-born neurons but such currents were small and thus a minor component of the response. Furthermore, we found preliminary evidence that adult-born GCs (or radial glia) may themselves release both GABA and glutamate that act on mature GCs.

The importance of these findings for information processing in the intact DG circuit was demonstrated by stimulating adult-born GCs in awake, behaving animals and showing that this decreased the total number of GCs activated by exploration of a novel environment. Importantly when an analogous experiment was conducted with mice in which ChR2 was expressed in predominately mature GCs no alteration in the number of c-Fos labeled GCs was observed. Transgene induction in Arc-ChR2 mice resulted in a similar number of GCs expressing ChR2 to Nestin-ChR2 mice, although we cannot be certain an exactly matched number of GCs were activated *in vivo*. These results indicate that *in vivo* there is a net inhibitory effect of young adult-born GCs on mature GCs, and suggest that this effect is more pronounced than the inhibitory feedback evoked by mature GC activity.

IPSCs were robustly induced when optical stimulation was given at frequencies corresponding to physiologically relevant firing rates. Moreover, the depression in evoked synaptic currents during trains of stimulation was stronger for EPSCs than IPSCs, so that inhibition increasingly dominated in such a scenario. While we acknowledge that simultaneous optogenetic activation of a cohort of cells represents an artificial stimulus, IPSCs were: 1) maintained over prolonged light stimulation when adult-born neurons would have fired randomly and very likely asynchronously, and 2) evoked by stimuli of very low light intensity, where only a small fraction of adult-born neurons would have been recruited.

Ongoing neurogenesis (Zhao et al., 2008; Ming and Song 2011; Drew et al., 2013) and sparse activity (i.e. the firing of only a very low proportion of GCs at any one time (Jung and McNaughton, 1993; Chawla et al., 2005; Neunuebel and Knierim, 2012) are hallmarks of the DG and both have been hypothesized to be pivotal to its function (see Drew et al., 2013). The role we suggest here for adult-born GCs in regulating activity in inhibitory interneurons in the DG and thus influencing mature GC activity suggests a potentially important link between these two properties.

The maintenance of sparse activity depends on both intrinsic properties of mature GCs (in particular, their strikingly hyperpolarized resting potentials, see Spruston and McBain, 2007) and on robust synaptic and extrasynaptic inhibition (Coulter and Carlson, 2007; Yu et al., 2013). Consistent with dynamic inhibition being important for DG information processing, single unit recordings *in vivo* by Nitz and McNaughton (2007) showed that, in contrast to CA1 where interneurons' firing rates decreased, spiking in DG interneurons markedly and rapidly increased when an animal encountered new surroundings. Interestingly, mice lacking adult hippocampal neurogenesis have deficits in encoding novel contexts specifically when exposure to those contexts is brief (Drew et al., 2010).

Another pertinent behavioral study is that of Burghardt et al. (2012) that investigated the requirement of adult neurogenesis for cognitive flexibility in a spatial learning task. Mice moving on a rotating disk had to learn to avoid a stationary shock zone (defined by static distal cues) and then adjust their escape behavior when the shock zone was moved. Ablated mice learned the task at control levels but when the shock zone was changed showed a pronounced deficit in escape behavior. Interestingly, after the reversal learning trials immunohistochemical analysis revealed that ablated animals had significantly more mature GCs expressing the IEG ARC in the dorsal DG. Hence, ablating neurogenesis induced a behavioral deficit that correlated with an increase in the number of GCs activated specifically when an animal had to distinguish between a new mnemonic demand and a previously learned rule.

This study suggests that adult-born GCs may function in selecting or suppressing mature GCs involved in a previous memory to allow a new memory to be formed (or acted upon) more readily. This is of particular interest when compared to our observation that stimulating adult-born GCs *in vivo* decreased the number of mature GCs activated during

exploration; a manipulation that also causes memory encoding deficits (in Danielson et al., submitted).

Also of direct relevance to our current results is a study that found gamma oscillations, occurring in discrete bursts in the DG of anaesthetized mice, were larger when adult neurogenesis had been ablated (Lacefield et al., 2012). Gamma oscillations represent coordinated firing of PV-expressing basket cells (Bartos et al., 2007) and thus this observation suggests that adult-born GCs change the dynamics of activity in GABAergic basket cells and that this may have important ramifications for overall DG activity patterns.

Recently, a number of studies have explored the role of adult-born GCs in regulating overall network activity. Ikrar et al. (2013) observed that altering neurogenesis levels bidirectionally affected overall DG excitability—as assayed with voltage-sensitive dye signals evoked by GC layer stimulation—consistent with adult-born GCs having an overall inhibitory function. Moreover, an *in vivo* study of EPSP:spike coupling in the DG has shown that in mice where adult neurogenesis was ablated, input:output coupling was enhanced (Park et al., 2015). Our results suggest a direct and strong input to GABAergic interneurons by adult-born GCs which may account for these observations. Future studies will be required to dissect precisely which cell types adult-born GCs innervate (which may vary during their development), as this will indicate how they might modulate activity in all other cell types of the DG. Important too, will be a careful comparison of this innervation pattern to that of mature GCs.

Here, though, we also provide evidence that feedback inhibition resulting from activation of a similarly sized population of mainly mature GCs does not inhibit overall population activity in the DG as assayed by IEG expression. Interestingly, optically evoked IPSCs in slices from such animals were not (despite a trend) significantly smaller than those seen in Nestin-ChR2 mice. This suggests that it may be the combination of robust coupling to inhibitory circuits plus the higher excitability of young adult-born GCs that underlies their net inhibitory function. Notably, fast synaptic GABAergic input is one of the last properties to develop in adult-born GCs (Espósito et al., 2005). This late maturation contributes to these cells preferential recruitment by afferent drive (Marin-Burgin et al., 2012) but it would also indicate that these neurons themselves would be unaffected by the activation of GABAergic neurons that they induce.

Finally, further support for an important inhibitory function of adult-born GCs comes from work we recently published showing that the severity of kainic acid-induced seizures was greater in mice in which adult neurogenesis had been ablated, therefore suggesting that these neurons help restrain runaway excitation in pathological conditions (Iyengar et al., 2015).

Another study published while this paper was under review concluded, however, that coupling to inhibitory networks is a late event in the ontology of adult-born GCs (Temprana et al., 2015). This study used retroviruses to express ChR2 in adult-born GCs of specific ages; the recruitment of inhibition by adult-born GCs was weak 4 weeks post-mitosis, but strong 7 weeks after mitosis - a cell age that was defined as mature. Our study stimulated a cohort of cells ranging in age from 0 to 6–7 weeks post-mitosis, and it may well be that it was the more mature cells in this cohort that were responsible for the bulk of synaptic inhibition that we observed. Hence, the importance of inhibitory drive induced by adult-born GCs might be underestimated by Temprana et al. (2015) due to a distinct definition of immature. The physiology of adult-born hippocampal neurons changes significantly between four and seven weeks post-mitosis (see Zhao et al., 2008; Ming and Song 2011; Drew et al., 2013). Our rationale for choosing the 6–7 week time point was that behavioral studies indicate that adult-born neurons make unique contributions to cognition in a window 4-6 weeks post-mitosis but not during the first four weeks (Denny et al., 2012; see also Drew et al., 2013). This later window, up to around 6 weeks post-mitosis, may therefore be unique in that the neurons have overlapping hyperexcitability, robust excitatory cortical drive, weak inhibitory GABAergic input and robust output to local interneurons.

In addition to adult-born GCs activating GABAergic interneurons, we also found evidence suggesting that adult-born neurons may release GABA and glutamate directly onto mature GCs. Rather than being ablated, optically evoked IPSCs were reduced by 75% by glutamate receptor antagonists to reveal a direct GABAergic current, whereas blockade of $GABA_A$ receptors and of AMPA receptors (to prevent synaptic excitation of postsynaptic neurons) revealed a glutamatergic current mediated by high affinity NMDA glutamate receptors. GABA release was dependent on voltage-gated sodium channel function and influx of extracellular calcium.

There is a significant, if sometimes controversial, literature suggesting that immature GCs in the developing brain co-release GABA and glutamate (at least onto CA3 pyramidal neurons) (Walker et al., 2001; Gutiérrez, 2005; Beltrán and Gutiérrez, 2012, but see Uchigashima et al., 2007; Cabezas et al., 2012). As for immature GCs born in the adult brain, immunohistochemical analysis (Lara et al., 2012) showed expression of the GABA-synthesizing enzyme GAD-67 in their mossy fiber terminals (but not in the cell body) whereas immature GCs (isolated via their expression of a GAD-67-GFP transgene) expressed markers consistent with a functional GABAergic phenotype (Cabezas et al., 2013). Analysis of the latencies of direct GABAergic responses showed them to be variable compared to IPSCs evoked by optical stimulation of PV-expressing interneurons, suggesting that coupling between excitation and release may be variable in developing adult-born GCs or that volume transmission of GABA (Markwardt et al., 2011) is involved.

IPSCs evoked by optical activation of adult-born GCs and recorded in mature GCs by Temprana et al. (2015) were ablated by glutamate receptor antagonists, indicating that no GABA was released directly from the ChR2-expressing neurons onto mature GCs. Additionally, no optically evoked EPSCs were observed. These differences may be due to the distinct cell populations – in terms of cell-age and the inclusion here of radial glial cells—expressing ChR2 and potentially the

intactness of microcircuits within coronal versus horizontal hippocampal slices. More work is required to resolve these differences.

Because a recent report raised concerns about off-target recombinase activity in Nestin-CreER^{T2} mouse lines, which varied according to the reporter strain used (Sun et al., 2014), we performed a number of control studies. In our experimental groups, a small number of ChR2eYFP-positive cells were occasionally apparent in the hilus which may represent ectopic expression or abnormal adult-born GC migration (McCloskey et al., 2006; Myers et al., 2013). When we specifically looked for markers of an interneuron phenotype (i.e. immunoreactivity for GAD-67 or PV) or a mossy cell identity (i.e., calretinin immunoreactivity) we found no overlap with ChR2-eYFP expression. We also examined optically evoked currents in aged mice where neurogenesis levels are extremely low and in mice that were focally X-irradiated to kill dividing cells and young neurons. IPSCs evoked under control conditions were substantially reduced by both manipulations. Critically for direct GABA release on to mature GCs, direct IPSCs (recorded after glutamate receptor blockade) were 75% smaller following X-irradiation, consistent with them being primarily mediated by adult-born neurons. The fact that synaptic currents were not entirely abolished is consistent with the observation that ChR2-eYFP-positive cells were sometimes still apparent in the GCL suggesting ablation was incomplete and/or that living in an EE can facilitate any residual capacity for neurogenesis after irradiation (Fan et al., 2007).

EPSCs were significantly reduced by X-irradiation. This is in contrast to a lack of effect of aging on EPSC amplitudes. We note, however, that the aging experiment was conducted in standard housed animals, in which EPSCs were always small, suggesting that a very low baseline EPSC is present that is not diminished by advancing age. Therefore, we cannot exclude that other non-neurogenesis dependent effects also contribute to the EPSC amplitude. By contrast, the X-irradiation experiment was conducted in EE animals. Although the effect of EE on EPSCs *per se* was not statistically significant ($P = 0.068$), the reduction of average EPSC amplitude by irradiation suggests that in EE animals adult-born GCs contribute to the generation of excitatory input to mature GCs.

Overall, the present study provides a robust demonstration that adult-born GCs can evoke inhibition onto mature GCs in the DG. This work therefore suggests that rather than acting solely as independent encoding units, young adult-born GCs, with their unique physiological properties, will act to modulate overall GC activity levels (Sahay et al., 2011; Piatti et al., 2013). From the current findings, two working hypotheses arise:

1. Adult-born GCs make an essential contribution to the degree or timing of inhibition so as to globally modulate the activity of mature GCs. This hypothesis predicts that in experiments combining real-time monitoring of mature GC activity *in vivo* (Leutgeb et al., 2007; Dombeck et al., 2010; Neunuebel and Knierim, 2012) and an ability to selectively block activity in adult-born GCs, a change in the firing patterns of mature GCs will be observed when adult-born neurons are silenced. Potential effects would range from a frank disinhibition of mature GCs to a shift in phase locking to local network oscillations, which themselves might be altered by such a manipulation (Lacefield et al., 2012). Such effects may depend on the context in which silencing is applied, i.e. on what cognitive demands the animal faces at the time (Burghardt et al., 2012). Of note, the study by Park et al. (2015) showed that learning-dependent shifts in EPSP:spike coupling were severely disrupted in mice in which neurogenesis had been ablated.
2. Dynamic rewiring of DG connectivity is an important function of adult neurogenesis and the innervation of local interneurons by adult-born GCs is an important aspect of this process. Incoming presynaptic termini of adult-born neurons take over postsynaptic sites previously occupied by mature GCs on CA3 pyramidal neurons (Toni et al., 2008) and learning induces altered connectivity between GCs and CA3 interneurons (Ruediger et al., 2011). The addition of new GCs over time may contribute to remodeling of GC-interneuron connectivity in the DG that influences which mature GCs are likely to be coactivated, i.e., it would facilitate the creation of new and distinct DG representations.

This study emphasizes that to understand the function of adult hippocampal neurogenesis assessing its impact on processing within, and not just through, the DG is required.

METHODS

All reagents were from Sigma-Aldrich Chemical Co. (St. Louis, MO) unless otherwise stated and all animal procedures were approved by the IACUC of The New York State Psychiatric Institute.

Animals

Experimental animals were heterozygous for a floxed-stop ChR2-eYFP transgene (AI32; Madisen et al., 2012) and hemizygous for a Cre-recombinase transgene. These animals were generated by crossing mice homozygous for the ChR2-eYFP gene with mice that carried one copy of the Cre transgene. In experiments examining adult-born GCs, a Nestin-CreER^{T2} transgene (Dranovsky et al., 2011) was employed. To activate Cre-recombinase activity, mice at 6–8 weeks of age were administered Tamoxifen (TMX) for five consecutive days [3 mg per day in 150 μl vehicle (10% ethanol, 90% corn oil) i.p.]. The fifth day was designated post-induction day 0. In some experiments the floxed-stop ChR2-eYFP line was crossed to a proopiomelanocortin (POMC)-Cre line (to target all GCs, McHugh et al., 2007) or a PV-Cre line (to target PV-expressing interneurons, Lovett-Barron et al., 2012); these were non-inducible Cre lines where ChR2-eYFP induction occurred during development. (These

TABLE 1.

Summary of Mice Used in this Study

Figure	Experiment	Control group Housing, sex, (# mice, # slices/neurons)	Experimental group Housing, sex, (# mice, # slices/neurons)	Notes
1c-d	Characterisation	Immunohistochemistry: SH, M (3-4, n/a)	Electrophysiology: EE, F (2, 4)	–
2a-d	Effect of housing	SH, F (5, 28)	EE, F (7, 40)	Littermates
2e-f	Effect of cell-age	EE, F (7, 40) (as in 2a-d)	EE, F (4, 15)	
3a-c	IPSC:EPSC ratios	n/a	EE, F (5, 10)	–
3d-g	Stimulus parameters	SH, F (3-4, 5-7)	EE, F (4-7, 5-16)	Subset of animals from Fig. 2a-e
4a-c	GluR Blockade	50 ms: EE, F (6, 14)	2 ms: EE, F (4, 10)	50 ms from Fig. 2a-d, 2 ms from Fig. 3a-c
4d-e	TTX/0 Calcium	TTX: EE, F (4, 5)	0 Ca: EE, F (4, 5)	Also used for Fig. 3a-c
5	X-irradiation	Sham: EE, F (3, 16)	X-ray: EE, F (3, 18)	Littermates
6a-c	*In vivo*, c-Fos induction in Nestin-ChR2 mice	Vehicle: SH, M (7, n/a)	TMX: SH, M (5, n/a)	Littermates
6d-e	*In vivo*, c-Fos induction in Arc-ChR2 mice	Cre-negative: SH, M (6, n/a)	Cre-positive: SH, M (4, n/a)	Littermates
S1b-c	Double-labeling	SH, F (3, n/a)		
S1e	Antagonists	SR 95531: EE, F (4,10)	NBQX+APV: EE, F (4, 10)	–
S2, S5	Double-labeling	EE, F (3, n/a)	–	–
S3	Stimulus parameters	As for Fig. 3		–
S4a-c	POMC- and PV-Cre	POMC: SH, F (3, 11)	PV: SH, F (2, 8)	–
S4c-d	Latencies	+ a subset of Figs. 2a–d		
S6	Effect of animal age	14 weeks: SH, F, (2, 12)	35 weeks: SH, F (2, 12)	Induced & recorded in parallel
S8	*In vivo*, c-Fos induction	As in Figs. 6a–c		
S9	*In vivo*, c-Fos induction	As in Figs. 6d,e		
S10	IPSCs and EPSCs in Arc-ChR2 mice	As in Figs. 2a–d (EE grp)	Arc-ChR2: EE, F (2, 13)	–

Abbreviations: SH - standard housing, EE - enriched environment, M - male, F - female, TTX - tetrodotoxin, NBQX - 2,3-dihydroxy-6-nitro-7-sulfamoyl-benzo[f]quinoxaline-2,3-dione, APV - (2*R*)-amino-5-phosphonovaleric acid, GluR - glutamate receptor, POMC - proopiomelanocortin, PV - parvalbumin, TMX - Tamoxifen.

animals were all housed in standard conditions.) Our breeding strategy resulted in mice that were of mixed strains (C57BL/6 and 129S6/SvEvTac); therefore littermate controls were used for specific experiments. We also used Arc-CreER^{T2} mice (Denny et al., 2014). Littermate controls without the Cre allele were used as controls. To induce a sparse pattern of transgene expression in the DG, six week old mice were given a single IP TMX injection and then exposed to the conditioning phase of a fear-conditioning protocol and then left for three weeks to allow robust ChR2-eYFP expression (see Denny et al., 2014). Table 1 summarizes all mice used in this study.

SH was an 18 cm × 30 cm Perspex cage (i.e. a standard mouse cage) containing three to five mice. EE consisted of two 24 cm × 45 cm cages joined by a plastic tube, which housed five to eight mice and contained four running wheels, plastic igloos, plastic tubes and nesting material. Mice were born and reared in SH and then either maintained there (as groups of three to five after weaning) or placed in EE at TMX administration as indicated in the *Results* section. Female mice were used for all physiology experiments as male mice living in EE are typically aggressive toward each other. However, the experiment in Figure 5 and immunohistochemical characterisation in Figure 1 used male mice.

Hippocampal irradiation was conducted as previously described (Denny et al., 2012, 2014). Briefly, after sodium pentobarbital (6 mg/kg, i.p.) anaesthesia, mice were placed in a stereotaxic frame, and cranial irradiation applied using a XRAD320 system (Precision Xray Inc.) operated at 300kV and 12mA. A 4 × 14-mm window above the hippocampus in a lead plate that otherwise shielded the entire body and most of the head allowed for focal X-ray application. X-rays were filtered using a 2mm Al filter and the source to skin distance was 36 cm. A cumulative dose of 7.5 Gy was given via three 2.5 Gy doses delivered over 2 minutes and 40 seconds on days 1, 4, and 7. In the text, the time after X-irradiation is the time after the first day.

Slice Physiology

Mice were anaesthetized by halothane or Isoflurane (Webster Veterinary) inhalation and then decapitated. Brains were rapidly removed and placed in ice-cold dissection solution (in mM, sucrose 195, NaCl 10, KCl 2.5, NaH_2PO_4 1, $NaHCO_3$ 25, glucose 10, $MgCl_2$ 6, $CaCl_2$ 0.5). 370 μm thick horizontal slices were cut on a vibratome (VT1000S; Leica). Slices from either extreme of the dorsoventral axis were discarded, and hemisected slices were placed in recovery solution (a 50:50 mix of dissection and recording solutions) and kept at 37°C for 30 minutes and then at room temperature until use. Recordings were made at 30–32°C (TC324-B; Warner Instrument Corp) in ACSF (in mM, NaCl 124, KCl 2.5, NaH_2PO_4 1, $NaHCO_3$ 25, glucose 20, $MgCl_2$ 1, $CaCl_2$ 2), using infrared-differential interference contrast (IR-DIC) optics on an upright microscope (Axioskop-2 FS; Zeiss) using an amplifier (Multiclamp 700B), digitizer (Digidata 1322A) and Clampex 10.2 software (all Molecular Devices). Patch pipettes were made from borosciliate glass (A-M Systems) using a micropipette puller (Model P-1000; Sutter Instruments). In the bath, initial pipette resistance was 4.5–6.5 MΩ. Recordings were made without correction for junction potentials. For voltage-clamp recording, a caesium-based internal solution was used (in mM Cs-methanesulphonate 125, NaCl 4, HEPES 10, EGTA 1, MgATP 4, Na_2GTP 0.3 Na-phosphocreatine 10, QX 314-Cl 5). Current-clamp recordings (i.e., Fig. 1d) employed a potassium-based solution (in mM, K-methanesulphonate 130, KCl 10, NaCl 4, HEPES 10, EGTA 0.1, MgATP 4, Na_2GTP 0.3 Na-phosphocreatine 10). As the vast majority of GCs in the outer GCL are mature perinatally born cells (e.g. Dranovsky et al., 2011), only neurons from the outer one-third of the GCL were targeted for recording of mature GCs. Immediately after breakthrough, the input resistance (IR) of all neurons was assessed. Immature adult-born GCs have very high IRs (>1GΩ), which fall to mature values (~200-300 MΩ) across approximately four week, e.g. see Mongiat et al. 2009), whereas a basket cell has a very low input resistance (50-100 MΩ (Scharfman, 1995b) or lower (Buhl et al., 1996)). No neuron used in this study had an IR of > 500 MΩ or <100 MΩ. A randomly selected subset of neurons used herein had an average IR of 260.9 ± 16.5MΩ ($n = 32$).

For optical stimulation, a 200 μm diameter, 0.37 numerical aperture multimode fiber (Thorlabs) was connected by a patch cord to a 100 mW 473 nm laser (OEM Laser Systems). Recordings were made near the apex of the DG and from both the upper and lower blades with no detectable differences so results were pooled. Multiple slices from the same mouse were used, but only one neuron per slice. The fiber optic was held by a micromanipulator at approximately 30° to the surface of the slice, above the tip of the granule cell layer of the blade in which the recorded neuron was situated. 15–20 mW light intensity at the fiber tip was used for all slice experiments (except those in Figs. 2f,g), hence, light intensity was supramaximal (see Fig. 2g). In some experiments (Fig. 4g), a bipolar stimulating electrode (FHC) was positioned on the outer two-thirds of the molecular layer to electrically evoke synaptic inputs. Stimuli were monopolar current pulses (triggered at 0.05 Hz) controlled by a stimulus isolator (ISO-flex, AMPI Instruments) and Clampex 10.2 software.

In Vivo Optical Stimulation

Mice were administered TMX or vehicle as described above, and 1 week later were implanted with indwelling fiber optics bilaterally targeted to the dorsal DG (1.5 mm anterior-posterior, 1 mm medio-lateral, 1.7 mm depth below dura, as in Kheirbek et al. (2013); see Sparta et al. (2012) for detailed methods). Seven weeks after induction they were tested behaviourally. Mice explored a novel environment (an "open-field" chamber 56 cm wide × 56 cm long × 40 high (Kinder Scientific) in low-light conditions: 16-20 lux) for 10 minutes with blue light pulses (20 ms duration at 10 Hz) delivered throughout the time in the new environment. They were returned to their home cages for 80 minutes, then deeply anaesthetized with i.p. ketamine/xylazine before transcardial perfusion with ice-cold phosphate buffered saline (PBS) followed by 4% paraformaldehyde (PFA) in PBS.

Immunohistochemistry

Brains were post-fixed for 24 hours in 4% PFA in PBS and then transferred to PBS containing 30% sucrose (at 4° for approximately 36 hours) prior to sectioning at 35 μm on a cryostat (CM 3050S; Leica). Immunohistochemistry was performed as previously described (Denny et al., 2014). Primary antibodies were: chicken anti-green fluorescent protein (GFP; 1:500, Abcam, Figs. 1, 5 and Supporting Information Fig. S6), goat anti-doublecortin (DCX; 1:500, Santa Cruz Biotechnology, Fig. 1 and Supporting Information Fig. S4), rabbit anti-c-Fos (1:5000, Calbiochem, Fig. 5 and Supporting Information Fig. S6), rabbit anti-Ki67 (1:100, Vector) and mouse anti-NeuN (1:1500, Millipore). Secondary antibodies were: biotinylated donkey anti-chicken (Figs. 1, 5 and Supporting Information Fig. S6), Cy3-AffiniPure donkey anti-goat (Fig. 1), Cy3-AffiniPure donkey anti-rabbit (Fig. 5 and Supporting Information Fig. S6), and biotinylated anti-goat (Fig. 1 and Supporting Information Fig. S4) (all 1:250 after dilution in glycerol; all Jackson Immunoresearch Labs). For visualisation, streptavidin-Cy2 was used (1:125 after dilution in glycerol, Jackson Immunoresearch Labs, Figs. 1, 5 and Supporting Information Fig. S6) or the Vectastain ABC Kit (Vector labs, Fig. 1 and Supporting Information Fig. S4). Animals used for example images in Figure 1 and Supporting Information Figure S4 were from the same Nestin-ChR2 mouse colony as all other experiments.

For immunohistochemical characterisation of ChR2-eYFP$^+$ cells, confocal scans (FluoView1000; Olympus) of DG sections were taken at 40×. For calculating recombination efficiency, 35 μm sections were cut and four sections spanning the full dorsoventral axis (~600 μm between sections) were assessed. 100 DCX cells were counted from these four sections along the dorsoventral axis. These cells were then classified as positive or negative for ChR2-eYFP. To sample the phenotypes of

ChR2-eYFP$^+$ cells, 35 μm sections were cut, and two sections/mouse (≈1200 μm between sections, one dorsal and one medioventral section) were imaged by taking confocal stacks at 40×. To calculate the percentage of ChR2-eYFP$^+$ cells that expressed Ki67, DCX or NeuN, the total ChR2-eYFP$^+$ cells in 300 μm × 200 μm region of interest in the upper blade of the DG were counted in the green channel, and then in the red channel the numbers of ChR2-eYFP$^+$ cells immunoreactive for DCX, Ki67 or NeuN were counted.

For Supporting Information Figures S2 and S5, the antibodies used were: chicken anti-YFP (1:1000, Abcam), mouse anti-GAD-67 (1:2000, EMD Millipore), mouse anti-PV (1:1000, EMD Millipore) and rabbit anti-calretinin (1:500, EMD Millipore). Secondary antibodies were Alexa Fluor 488-goat anti-chicken (1:400), Alexa fluor 546-donkey anti-mouse (1:500) and Alexa fluor 568 donkey anti-rabbit (1:500; all Life Technologies). From three animals - three sections per mouse - GAD-67 and PV positive cells were counted from the hilus and GCL and calretinin positive cells from the hilus only, and the number of such cells that contained ChR2-eYFP counted.

To quantify c-Fos expressing cells, 35 μm sections were cut and every sixth coronal section of the hippocampus was chosen and the total number of c-Fos positive cells in the GC layer in one hemisphere from each section was counted. To compare the number of ChR2-eYFP-positive cells in Nestin-ChR2 and Arc-ChR2 mice, sections were processed in parallel and the number of positive cells in a 200 × 300 μm field of view were counted.

Data Analysis

Electrophysiological data were analysed using Clampfit 10.2 software (Molecular Devices) and Sigmaplot 12.0 (Systat) for constructing graphs and statistical comparisons. The peaks of evoked membrane currents were detected automatically using Clampfit10.2 software; a neuron was classified as positively responding to a light stimulus if evoked currents were phase-locked to the stimulus and were >10pA in amplitude with the kinetic profile of a synaptic response. Latencies were measured manually as the time after the beginning of the light pulse that there was a clear upward deviation of the holding-current. Area under the curve was used to measure charge transfer. Example traces are of single responses. Statistical analyses were used as indicated in the figure legends, where data failed normality tests non-parametric tested were used; statistical significance was set at $P < 0.05$.

ACKNOWLEDGMENTS

The authors thank Elizabeth Maier Balough for technical assistance and Gregg Crabtree for discussion. They are grateful to Hongkui Zeng for AI32 mice and Attila Losonczy and Boris Zemelman for PV-Cre mice. RH consults for Lundbeck, Servier and Roche. All other authors declare no competing interests.

REFERENCES

Bartos M, Vida I, Jonas P. 2007. Synaptic mechanisms of synchronized gamma oscillations in inhibitory interneuron networks. Nat Rev Neurosci 8:45–56.

Beltrán JQ, Gutiérrez R. 2012. Co-release of glutamate and GABA from single, identified mossy fiber giant boutons. J Physiol 590: 4789–4800.

Bruel-Jungerman E, Laroche S, Rampon C. 2005. New neurons in the dentate gyrus are involved in the expression of enhanced long-term memory following environmental enrichment. Eur J Neurosci 21:513–521.

Buhl EH, Szilágyi T, Halasy K, Somogyi P. 1996. Physiological properties of anatomically identified basket and bistratified cells in the CA1 area of the rat hippocampus in vitro. Hippocampus 6:294–305.

Burghardt NS, Park EH, Hen R, Fenton AA. 2012. Adult-born hippocampal neurons promote cognitive flexibility in mice. Hippocampus 22:1795–1808.

Cabezas C, Irinopoulou T, Gauvain G, Poncer JC. 2012. Presynaptic but not postsynaptic GABA signaling at unitary mossy fiber synapses. J Neurosci 32:11835–11840.

Cabezas C, Irinopoulou T, Cauli B, Poncer JC. 2013. Molecular and functional characterization of GAD67-expressing, newborn granule cells in mouse dentate gyrus. Front Neural Circuits 7:60.

Chawla MK, Guzowski JF, Ramirez-Amaya V, Lipa P, Hoffman KL, Marriott LK, Worley PF, McNaughton BL, Barnes CA. 2005. Sparse, environmentally selective expression of Arc RNA in the upper blade of the rodent fascia dentata by brief spatial experience. Hippocampus 15:579–586.

Coulter DA, Carlson GC. 2007. Functional regulation of the dentate gyrus by GABA-mediated inhibition. Prog Brain Res 163:235–243.

Danielson N, Kaifosh P, Zaremba JD, Lovett-Barron M, Tsai J, Denny CA, Balough EM, Goldberg A, Drew LJ, Losonczy A, Hen R, Kheirbek MA. Distinct contributions of adult-born hippocampal granule cells to memory encoding. (submitted).

Denny CA, Burghardt NS, Schachter DM, Hen R, Drew MR. 2012. 4- to 6-week-old adult-born hippocampal neurons influence novelty-evoked exploration and contextual fear conditioning. Hippocampus 22:1188–1201.

Denny CA, Kheirbek MA, Alba EL, Tanaka KF, Brachman RA, Laughman KB, Tomm NK, Turi GF, Losonczy A, Hen R. 2014. Hippocampal memory traces are differentially modulated by experience, time, and adult neurogenesis. Neuron 83:189–201.

Dombeck DA, Harvey CD, Tian L, Looger LL, Tank DW. 2010. Functional imaging of hippocampal place cells at cellular resolution during virtual navigation. Nat Neurosci 1:1433–1440.

Dranovsky A, Picchini AM, Moadel T, Sisti AC, Yamada A, Kimura S, Leonardo ED, Hen R. 2011. Experience dictates stem cell fate in the adult hippocampus. Neuron 70:908–923.

Drew MR, Denny CA, Hen R. 2010. Arrest of adult hippocampal neurogenesis in mice impairs single- but not multiple-trial contextual fear conditioning. Behav Neurosci 124:446–454.

Drew LJ, Fusi S, Hen R. 2013. Adult Neurogenesis in the Mammalian Hippocampus; Why the Dentate Gyrus? Learn Mem 20:710–729.

Espósito MS, Piatti VC, Laplagne DA, Morgenstern NA, Ferrari CC, Pitossi FJ, Schinder AF. 2005. Neuronal differentiation in the adult hippocampus recapitulates embryonic development. J Neurosci 25: 10074–10086.

Fan Y, Liu Z, Weinstein PR, Fike JR, Liu J. 2007. Environmental enrichment enhances neurogenesis and improves functional outcome after cranial irradiation. Eur J Neurosci 25:38–46.

Ge S, Yang CH, Hsu KS, Ming GL, Song H. 2007. A critical period for enhanced synaptic plasticity in newly generated neurons of the adult brain. Neuron 54:559–566.

Gu Y, Arruda-Carvalho M, Wang J, Janoschka SR, Josselyn SA, Frankland PW, Ge S. 2012. Optical controlling reveals time-dependent roles for adult-born dentate granule cells. Nat Neurosci 15:1700–1706.

Gutiérrez R. 2005. The dual glutamatergic-GABAergic phenotype of hippocampal granule cells. Trends Neurosci 28:297–303.

Houser CR. 2007. Interneurons of the dentate gyrus: An overview of cell types, terminal fields and neurochemical identity. Prog Brain Res 163:217–232.

Ide Y, Fujiyama F, Okamoto-Furuta K, Tamamaki N, Kaneko T, Hisatsune T. 2008. Rapid integration of young newborn dentate gyrus granule cells in the adult hippocampal circuitry. Eur J Neurosci 28:2381–2392.

Ikrar T, Fujiyama F, Okamoto-Furuta K, Tamamaki N, Kaneko T, Hisatsune T. 2013. Adult neurogenesis modifies excitability of the dentate gyrus. Front Neural Circuits 7:204.

Isaacson JS, Scanziani M. 2011. How inhibition shapes cortical activity. Neuron 72:231–243.

Iyengar SS, LaFrancois JJ, Friedman D, Drew LJ, Denny CA, Burghardt NS, Wu MV, Hsieh J, Hen R, Scharfman HE. 2015. Suppression of adult neurogenesis increases the acute effects of kainic acid. Exp Neurol 264:135–149.

Jung MW, McNaughton BL. 1993. Spatial selectivity of unit activity in the hippocampal granular layer. Hippocampus 3:165–182.

Kempermann G, Kuhn HG, Gage FH. 1997. More hippocampal neurons in adult mice living in an enriched environment. Nature 386: 493–495.

Kheirbek MA, Drew LJ, Burghardt NS, Costantini DO, Tannenholz L, Ahmari SE, Zeng H, Fenton AA, Hen R. 2013. Differential control of learning and anxiety along the dorsoventral axis of the dentate gyrus. Neuron 77:955–968.

Klempin F, Kempermann G. 2007. Adult hippocampal neurogenesis and aging. Eur Arch Psychiatry Clin Neurosci 257:271–280.

Lacefield CO, Itskov V, Reardon T, Hen R, Gordon JA. 2012. Effects of adult-generated granule cells on coordinated network activity in the dentate gyrus. Hippocampus 22:106–116.

Lara E, Beltrán JQ, Segovia J, Gutiérrez R. 2012. Granule cells born in the adult rat hippocampus can regulate the expression of GABAergic markers. Exp Neurol 237:134–141.

Leutgeb JK, Leutgeb S, Moser MB, Moser EI. 2007. Pattern separation in the dentate gyrus and CA3 of the hippocampus. Science 315:961–966.

Lovett-Barron M, Turi GF, Kaifosh P, Lee PH, Bolze F, Sun XH, Nicoud JF, Zemelman BV, Sternson SM, Losonczy A. 2012. Regulation of neuronal input transformations by tunable dendritic inhibition. Nat Neurosci 15:423–430.

Madisen L, Mao T, Koch H, Zhuo JM, Berenyi A, Fujisawa S, Hsu YW, Garcia AJ, 3rd Gu X, Zanella S, Kidney J, Gu H, Mao Y, Hooks BM, Boyden ES, Buzsáki G, Ramirez JM, Jones AR, Svoboda K, Han X, Turner EE, Zeng H. 2012. A toolbox of Cre-dependent optogenetic transgenic mice for light-induced activation and silencing. Nat Neurosci 15:793–802.

Marín-Burgin A, Mongiat LA, Pardi MB, Schinder AF. 2012. Unique processing during a period of high excitation/inhibition balance in adult-born neurons. Science 335:1238–1242.

Markwardt SJ, Dieni CV, Wadiche JI, Overstreet-Wadiche L. 2011. Ivy/neurogliaform interneurons coordinate activity in the neurogenic niche. Nat Neurosci 14:1407–1409.

McCloskey DP, Hintz TM, Pierce JP, Scharfman HE. 2006. Stereological methods reveal the robust size and stability of ectopic hilar granule cells after pilocarpine-induced status epilepticus in the adult rat. Eur J Neurosci 24:2203–2210.

McHugh TJ, Jones MW, Quinn JJ, Balthasar N, Coppari R, Elmquist JK, Lowell BB, Fanselow MS, Wilson MA, Tonegawa S. 2007. Dentate gyrus NMDA receptors mediate rapid pattern separation in the hippocampal network. Science 317:94–99.

Ming GL, Song H. 2011. Adult neurogenesis in the mammalian brain: Significant answers and significant questions. Neuron 70: 687–702.

Mongiat LA, Espósito MS, Lombardi G, Schinder AF. 2009. Reliable activation of immature neurons in the adult hippocampus. PLoS One 4:e5320.

Myers CE, Bermudez-Hernandez K, Scharfman HE. 2013. The influence of ectopic migration of granule cells into the hilus on dentate gyrus-CA3 function. PLoS One 8:e68208-

Neunuebel JP, Knierim JJ. 2012. Spatial firing correlates of physiologically distinct cell types of the rat dentate gyrus. J Neurosci 32: 3848–3858.

Nitz D, McNaughton B. 2004. Differential modulation of CA1 and dentate gyrus interneurons during exploration of novel environments. J Neurophysiol 91:863–872.

Park EH, Burghardt NS, Dvorak D, Hen R, Fenton AA. 2015. Experience-dependent regulation of the dentate gyrus excitability by adult-born granule cells. J Neurosci 35:11656–11666.

Piatti VC, Ewell LA, Leutgeb JK. 2013. Neurogenesis in the dentate gyrus: carrying the message or dictating the tone. Front Neurosci 7:50.

Ruediger S, Vittori C, Bednarek E, Genoud C, Strata P, Sacchetti B, Caroni P. 2011. Learning-related feedforward inhibitory connectivity growth required for memory precision. Nature 473:514–518.

Sahay A, Wilson DA, Hen R. 2011. Pattern separation: A common function for new neurons in hippocampus and olfactory bulb. Neuron 70:582–588.

Sambandan S, Sauer JF, Vida I, Bartos M. 2010. Associative plasticity at excitatory synapses facilitates recruitment of fast-spiking interneurons in the dentate gyrus. J Neurosci 30:11826–11837.

Scharfman HE. 1995a. Electrophysiological evidence that dentate hilar mossy cells are excitatory and innervate both granule cells and interneurons. J Neurophysiol 74:179–194.

Scharfman HE. 1995b Electrophysiological diversity of pyramidal-shaped neurons at the granule cell layer/hilus border of the rat dentate gyrus recorded *in vitro*. Hippocampus 5:287–305.

Scharfman HE, Myers CE. 2013. Hilar mossy cells of the dentate gyrus: A historical perspective. Front Neural Circuits 6:106-

Sparta DR, Stamatakis AM, Phillips JL, Hovelsø N, van Zessen R, Stuber GD. 2012. Construction of implantable optical fibers for long-term optogenetic manipulation of neural circuits. Nat Protoc 7:12–23.

Spruston N, McBain C. 2007. Structural and functional properties of hippocampal neurons. In: Andersen P, Morris R, Amaral D, Bliss T, O'Keefe, editors. The Hippocampus Book. Oxford University Press, New York. pp. 133–202

Stone SS, Teixeira CM, Zaslavsky K, Wheeler AL, Martinez-Canabal A, Wang AH, Sakaguchi M, Lozano AM, Frankland PW. 2011. Functional convergence of developmentally and adult-generated granule cells in dentate gyrus circuits supporting hippocampus-dependent memory. Hippocampus 21:1348–1362.

Sun GJ, Sailor KA, Mahmood QA, Chavali N, Christian KM, Song H, Ming GL. 2013. Seamless reconstruction of intact adult-born neurons by serial end-block imaging reveals complex axonal guidance and development in the adult hippocampus. J Neurosci 33: 11400–11411.

Sun MY, Yetman MT, Lee TC, Chen Y, Jankowsky JL. 2014. Specificity and efficiency of reporter expression in adult neural proggentors vary substantially among nestin-CreER^{T2} lines. J Comp Neurol 522:1191–1208.

Swan AA, Clutton JE, Chary PK, Cook SG, Liu GG, Drew MR. 2014. Characterization of the role of adult neurogenesis in touch-screen discrimination learning. Hippocampus 24:1581–1591.

Temprana SG, Mongiat LA, Yang SM, Trinchero MF, Alvarez DD, Kropff E, Giacomini D, Beltramone N, Lanuza GM, Schinder AF. 2015. Delayed coupling to feedback inhibition during a critical

period for the integration of adult-born granule cells. Neuron 85: 116–130.
Toni N, Laplagne DA, Zhao C, Lombardi G, Ribak CE, Gage FH, Schinder AF. 2008. Neurons born in the adult dentate gyrus form functional synapses with target cells. Nat Neurosci 11:901–907.
Uchigashima M, Fukaya M, Watanabe M, Kamiya H. 2007. Evidence against GABA release from glutamatergic mossy fiber terminals in the developing hippocampus. J Neurosci 27:8088–8100.
van Praag H, Kempermann G, Gage FH. 1999. Running increases cell proliferation and neurogenesis in the adult mouse dentate gyrus. Nat Neurosci 2:266–270.
Walker MC, Ruiz A, Kullmann DM. 2001. Monosynaptic GABAergic signaling from dentate to CA3 with a pharmacological and physiological profile typical of mossy fiber synapses. Neuron 29:703–715.
Wang S, Scott BW, Wojtowicz JM. 2000. Heterogenous properties of dentate granule neurons in the adult rat. J Neurobiol 42:248–257.
Yu EP, Dengler CG, Frausto SF, Putt ME, Yue C, Takano H, Coulter DA. 2013. Protracted postnatal development of sparse, specific dentate granule cell activation in the mouse hippocampus. J Neurosci 33:2947–2960.
Zhao C, Deng W, Gage FH. 2008. Mechanisms and functional implications of adult neurogenesis. Cell 132:645–660.